JOURNAL OF AIRCRAFT
Vol. 38, No. 1, January–February 2001

Exploring the Feasibility of Pulsed Jet Separation Control for Aircraft Configurations

John C. Magill*
Physical Sciences Inc., Andover, Massachusetts 01810-1077
and
Keith R. McManus†
General Electric Corporate Research and Development Center, Niskayuna, New York 12309

This paper describes experiments aimed at demonstrating the effectiveness of pulsed vortex generator jets (PVGJs) in controlling separation on aircraft wings. The demonstration is accomplished by applying the jets to two relevant configurations and evaluating their effectiveness in a wind tunnel. The jet design and placement for both experiments was based on parametric studies described in a previous paper. In the first application, pulsed jets prevented separation over the wings on a three-dimensional lambda-wing fighter configuration at low speeds and high angles of attack. This experiment shows that the flow control method can enhance the lift, and hence the maneuverability, of advanced fighters in post-stall flight. The lambda-wing experiments also demonstrated that jets can be operated asymmetrically for lateral maneuvering control at high angles of attack. The second set of experiments tested higher speed ranges, applying jets to an airfoil section in an $M = 0.3$–0.5 flow. This configuration is relevant to subsonic cruise. The results show that PVGJs can increase lift and lift-to-drag ratios, but they were less effective at supercritical speeds where separation is induced by hinge line shocks. In all cases, the jets increased lift over their effective range although their drag effect was small.

Nomenclature

C_D, C_d	=	drag coefficient
C_L, C_ℓ	=	lift coefficient
C_{roll}	=	rolling moment coefficient
C_μ	=	momentum coefficient, $VR^2\rho_j(\pi D^2)\Delta N/4S\rho_\infty$
c	=	airfoil chord length
D	=	jet diameter
f_p	=	pulse frequency (Hz)
M_s	=	jet Mach number
M_∞	=	freestream Mach number
N	=	number of jets
S	=	wing area
Sr_c	=	Strouhal number, $f_p c/U_\infty$
U_∞	=	freestream velocity
VR	=	jet-to-freestream velocity ratio
α	=	angle of attack
Δ	=	duty cycle: fraction of pulse period over which jet is flowing
δ_{le}	=	leading-edge flap deflection angle
δ_{te}	=	trailing-edge flap deflection angle
ρ_j	=	jet exit density
ρ_∞	=	freestream density

Introduction

THIS paper describes a two-part experimental investigation aimed at demonstrating the feasibility of an advanced separation control technique for realistic aircraft configurations and flight conditions. Previous research explored the technique, pulsed vortex generator jets (PVGJs), and identified key operating parameters.[1–3] The wind-tunnel experiments addressed in this paper include measurements with a model lambda-wing/fuselage configuration representative of an advanced fighter and tests of a transonic airfoil with a leading-edge flap.

Active flow-control techniques are being pursued for the purpose of enhancing lift, reducing drag, and improving aerodynamic stability and control in future aircraft. The active systems will be used to enhance the performance of, or replace, traditional control actuators/surfaces presently in service. Potential applications span a broad range of vehicles, including next-generation fighters as well as heavy-lift transports. A principal goal in many flow-control studies is to develop an efficient actuator that is consistent with the stringent size, weight, and power requirements typical of flight-worthy components.

The present technique is the most recent in a progressive series of devices that delay separation by creating streamwise vortex structures over the wing upper surface. These structures mix high-energy air from the freestream to replace the boundary-layer fluid that has lost kinetic energy as a result of interaction with the surface. Thus, by energizing the upper-surface boundary layer, they supress stall.[4]

Predecessors to PVGJs have included the solid vortex generators[5,6] (VGs) in widespread use on commercial aircraft. Solid VGs are used primarily over inboard flapped wing sections. They have also been used to increase stall margins on light aircraft.

Several investigations have demonstrated that the vortex structures could be created with steady wall jets.[7–10] This technique could provide a greater effect than the solid vortex generators because the jets could penetrate further into the flow than the solid generators, and furthermore produce less drag. However, the jets require some source of air-mass flow, and the limited availability of air or the energy to pressurize it makes the steady jets less attractive.

The present work was aimed at finding a means to reduce the air flow required by jets while preserving their effectiveness for separation control. The flow-control technique described in this paper, shown schematically in Fig. 1, exploits the vorticity generation capabilities of impulsively started jets to enhance boundary-layer momentum transport. The effectiveness in suppressing stall is enhanced when the jet flow is made unsteady or pulsed.[1–3,11–17] This is due to both the enhanced vorticity production associated with the impulsively started jet flow[14] as well as the reduction in mass flow obtained because the jets are flowing for only some portion (10–50%) of the pulse cycle.

Received 29 October 1999; revision received 30 June 2000; accepted for publication 12 July 2000.

*Principal Research Engineer, 20 New England Business Center. Member AIAA.
†Mechanical Engineer, Mechanical Systems Laboratory. Member AIAA.

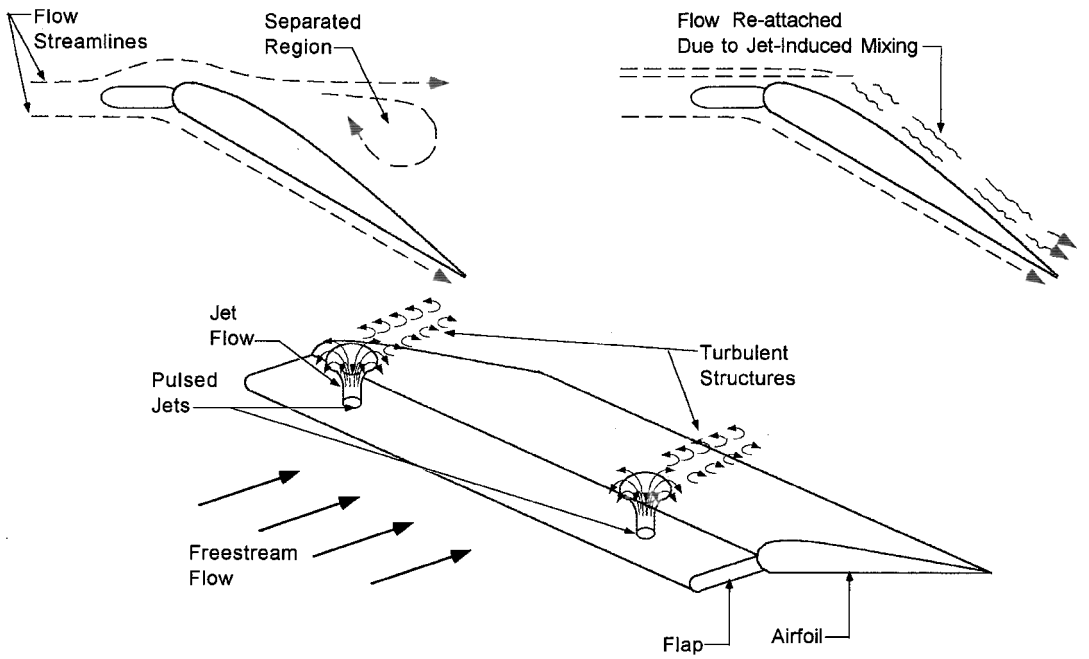

Fig. 1 Schematic diagram showing application of PVGJs on two-dimensional airfoil for separation control.

In addition to streamwise vortices, large-scale, turbulent vortex rings are generated in the flow when the jets are pulsed. Both types of structures can substantially increase cross-stream mixing and lead to stall suppression in adverse pressure gradients. The addition of pulsing has been shown to give good stall suppression with substantially lower jet-mass flow requirements than when the jets were operated with steady flow.

On an airfoil, jets are placed on a leading-edge flap. In high lift configurations, separation often occurs near the flap hinge line. The effectiveness of the jets is maximized if they are situated before the separation rather than in the wake.

This paper discusses the application of pulsed blowing systems on two models. The first set of wind-tunnel tests described was conducted with a three-dimensional aircraft model. The model resembles an advanced fighter configuration and has swept wings with the shape of Greek lambda symbols and, hence, is called a lambda-wing model. These experiments show that PVGJs improve lift on finite, swept wings and can also be used for lateral maneuvering control at high angles of attack.

The second of the two applications described employed a transonic airfoil with a leading-edge flap. Results will show that jets can delay separation in transonic flows. They increase both lift and lift-to-diag ratio, though their effectiveness is greater just below the critical Mach number than just above it, where hinge line shocks instigate separation. These results endorse the applicability of PVGJs to high subsonic cruise of transport aircraft.

The remainder of the paper is divided into two sections, each addressing one of the two experiments. The sections discuss the model configuration and the pulsed blowing system particular to each. Then results from wind-tunnel tests are presented. In both cases, the experiments demonstrated that PVGJs are effective in delaying stall, thus increasing peak lift and lift-to-diag ratio.

In the subsequent discussion, the operating conditions of pulsed jets are characterized using four parameters deemed important in previous studies: velocity ratio, duty cycle, Strouhal number, and momentum coefficient. The velocity ratio, designated VR, is the ratio of jet exit velocity to the wind-tunnel freestream velocity. The duty cycle, Δ, is the fraction of the pulse cycle during which the jet is flowing. It is given as a percentage in the text of this paper but is treated as a fraction when used mathematically. The Strouhal number Sr_c is defined by the relationship

$$Sr_c = f_p c / U_\infty$$

where U_∞ is the freestream velocity, c is the airfoil chord, and f_p is the pulse frequency in Hz. The momentum coefficient for the air flowing through the jets is defined as

$$C_\mu = VR^2 \times (\pi D^2/4S) \times \Delta \times N$$

It is useful for comparison the other flow control methods published by other researchers.

Prior work with flat plates and airfoil sections has shown that a particular range of parameters generally provided optimum separation control effect. Peak lift enhancement generally occurs near a Strouhal number $Sr_c = 0.5$. Lift enhancement generally saturates when the velocity ratio is increased beyond $VR = 4$. Prior investigations also showed that duty cycles of 25% produce the same effect as those of 50% for a given velocity ratio. Thus, 25% was chosen because it uses less air. These numbers were used as the design parameter sets for the two experimental efforts described in this paper.

Lambda-Wing Experiments

Model Description

The wind-tunnel model used in the first study is a generic tailless fighter configuration consisting of an ogive-cylinder fuselage with swept lambda wings (Fig. 2). The wing leading-edge sweep angle is 40 deg, and the airfoil cross-section is an NACA 65-006. The total wing span is approximately 83 cm, and the fuselage length is 111 cm. The mean aerodynamic chord of the inboard and outboard wing sections is 38 and 22.5 cm, respectively. The wings have both leading- and trailing-edge flaps with adjustable deflection. The length of the leading-edge flap corresponds to 9 and 16% of the mean aerodynamic chord of the inboard and outboard wing sections, respectively. Similarly, the trailing-edge flaps account for 18 and 31% of the chords.

The model was fitted with a pulsed blowing system to provide air pulses to actuator jets on the upper surfaces of the wing leading-edge flaps. There were four jets on each wing, and the locations of the jets along the leading edge are shown in Fig. 2. The jets were pitched 90 deg relative to the model axis and rolled toward the wing tip 45 deg from vertical. A modular valve system was designed to operate the pulsed jets for the lambda-wing model.

For the purpose of jet design, the wing was divided into two sections: the inboard (tapered) section and the outboard swept, constant chord section. The jet sizes and pulse frequencies were chosen for each section based on the mean aerodynamic chord for each of the

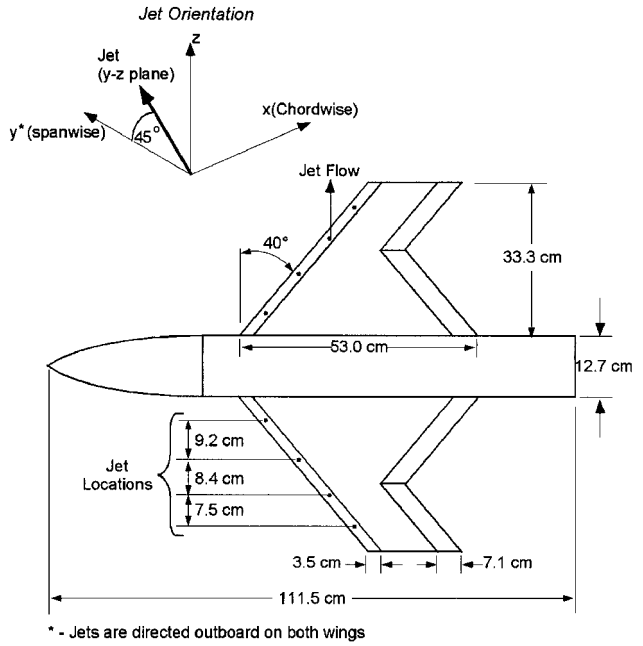

Fig. 2 Wind-tunnel model planform: lambda wing with ogive-cylinder fuselage.

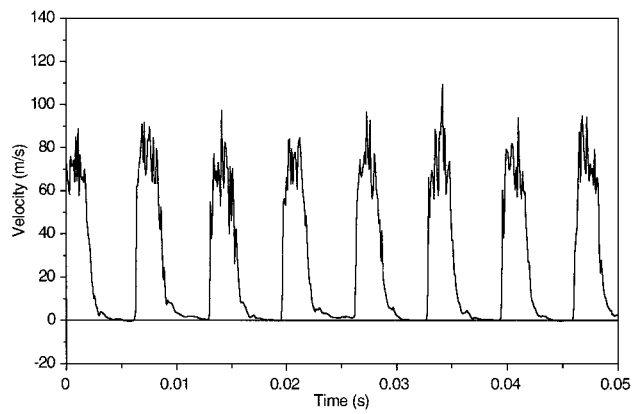

Fig. 3 Hot-film measurements of jet pulses for lambda-wing model.

two regions. The outer jets pulsed 50% faster than the inboard jets because the outboard section has a proportionally shorter chord. Thus, inboard and outboard jets had the same Strouhal number. The diameter of the jets was 3.2 mm on the inboard wing sections and 2.4 mm on the outboard sections. These jet sizes were determined from pulsed blowing performance-optimization studies on generic, two-dimensional wing models.[1–3]

The airflow for the pulsed jet system was individually metered to each wing by use of a mass flow controller (MKS Model 1559A) allowing maximum time-mean mass flowrates of 200 standard liters per minute (slpm) per wing. The pulse frequencies were continuously adjustable over a range from approximately 10 to 300 Hz. The system was controlled remotely from the wind-tunnel control room through an umbilical cord supplying the metered airflow and electrical signals to operate the high-speed valves.

Pulsed Valve Measurements

Before the wind-tunnel tests, the quality of the pulse shapes was verified. A hot-film anemometer placed at the exit of each jet measured the temporal velocity profile. Figure 3 shows the velocity profile for an inboard jet. A clear pulse train appears with minimal flow between pulses. All of the valves were identical in construction, except that the outboard valves were smaller, and the response shown here is characteristic of all of the actuator jets.

Wind-Tunnel Facility, Instrumentation, and Test Conditions

The model was tested in the Ohio State University 7 × 10 ft subsonic wind tunnel. Tests were performed with freestream velocities of $U_\infty = 33$ and 66 m/s corresponding to chord Reynolds numbers of 0.86 and 1.72×10^6 (per ft). The model was mounted on a sting support with angle-of-attack adjustment in the range of +5 to +40 deg. A six-component strain gauge balance was used to measure the forces and moments acting along and about the model body axes. A computer-automated system was used to acquire and digitize the balance-sensor signals and reduce them to force and moment coefficient form. Tare measurements were performed at all model orientations under wind-off conditions to correct for the influence of the model weight.

Discussion of Lambda-Wing Results

Baseline Aerodynamic Characteristics

Three different control surface configurations have been chosen to demonstrate the effects of PVGJs on the lambda-wing model lift and drag characteristics. The first two examples have a deflected leading edge flap ($\delta_{le} = 15$ and 30 deg) with no trailing-edge flap deflection, and the third example has a leading-edge flap deflection of $\delta_{le} = 30$ deg with a trailing-edge flap deflection of $\delta_{te} = 15$ deg. The first two example configurations represent those where moderate lift enhancement is desired for high-α maneuvering at relatively low speed. The third case represents a high lift configuration with both leading- and trailing-edge flaps deflected and is a typical configuration for landing approach. The baseline lift curves for the first two examples are shown in Fig. 4. That for the third case will be presented later.

Figure 4a shows baseline lift curves for the lambda-wing model for a freestream velocity $U_\infty = 66$ m/s and for two different leading-edge flap deflection angles. The data encompass the α range, where the lift curves roll over because of flow separation over the upper surface, then reach a maximum value, $C_{L\,max}$ and decrease as the wing stall becomes more severe. Both curves in Fig. 4 indicate that the wings stall smoothly without abrupt changes in slope. This is typical of low-aspect-ratio, highly swept wings. The maximum lift for the configurations shown is approximately 1.04 and 0.96 for leading-edge flap deflection angles, δ_{le}, of 30 and 15 deg, respectively. Baseline drag characteristics for the lambda-wing model are shown in Fig. 4b for the same flap configurations. The drag characteristics are approximately the same for the two cases with

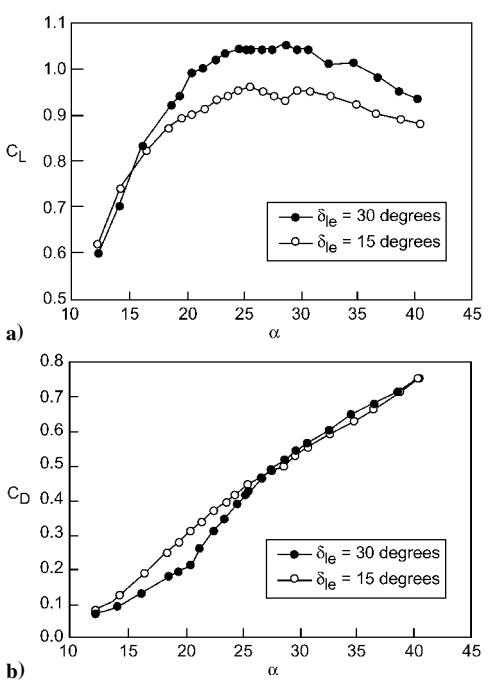

Fig. 4 Baseline lift (a) and drag (b) curves for lambda-wing model: U_∞ = 66 m/s, δ_{te} = 0.

$\alpha \geq 26$ deg; however, for $12 \leq \alpha \leq 25$ deg, the larger leading-edge flap deflection angle results in lower drag. This is most likely due to less severe flow separation over the upper surface.

Effects of PVGJs on Lambda-Wing Aerodynamic Characteristics

Experiments were conducted using the leading-edge PVGJ system to control separation over the wing upper surface at moderate to high α. The resulting effects on the model's aerodynamic performance were measured and are described below. Initial experiments were conducted using the PVGJ design operating conditions: $\Delta = 25\%$, $VR = 4$, $Sr_c = 0.5$. Using these jet pulse conditions as a starting point, the effects of the PVGJs on the lambda-wing aerodynamics were evaluated. These tests indicated relatively minor improvements in lift performance and suggested that the jet pulse parameters were not optimum. Tests were then performed to separately evaluate the effects of jet pulse amplitude and frequency on lift enhancement near $C_{L\,\max}$ and to determine optimum parameter ranges for the lambda-wing configuration.

Figure 5 shows the effect of varying pulse frequency on the lift coefficient while holding the jet amplitude fixed. Data are shown for two different freestream velocities and for $\alpha = 25$ deg, which corresponds to $C_{L\,\max}$ for the baseline case. The data for $U_\infty = 33$ m/s show that the lift enhancement due to the PVGJs increases with increasing jet pulse frequency up to a nondimensional frequency of $Sr_c \approx 1.0$, and then with further increases in frequency, the lift remains relatively flat. The data for $U_\infty = 66$ m/s support this trend up to $Sr_c = 1.0$; however, further increases in Sr_c for this freestream velocity were not possible because of limitations associated with the jet pulse valves. All subsequent tests using PVGJs were run using a nondimensional jet pulse frequency of $Sr_c = 1.0$.

The effects of varying jet pulse amplitude on the model lift coefficient are shown in Fig. 6. The data show that for very low PVGJ velocity ratios ($VR \leq 2$) there is a slight decrease in C_L. (This trend was found to be repeatable and also existed in data sets corresponding to other model configurations and $U_\infty = 33$ m/s.) Increasing VR beyond this value resulted in monotonically increasing lift values. Experiments at $U_\infty = 33$ m/s allowed higher values of VR to be tested and confirmed this trend. Within the available flow-rate range of the PVGJ system, increases in pulsed jet flow rate always resulted in increased control effectiveness.

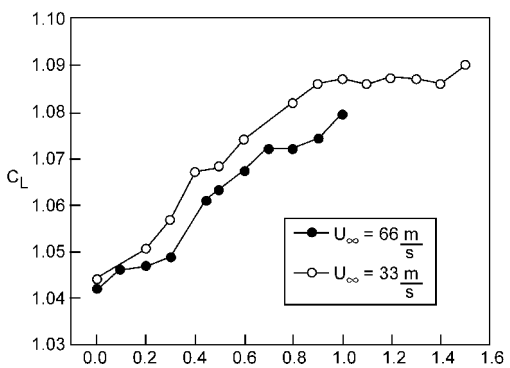

Fig. 5 Effect of jet pulse frequency on lift enhancement with PVGJs for two different freestream velocities: α = 25 deg, δ_{le} = 30 deg, VR = 5.

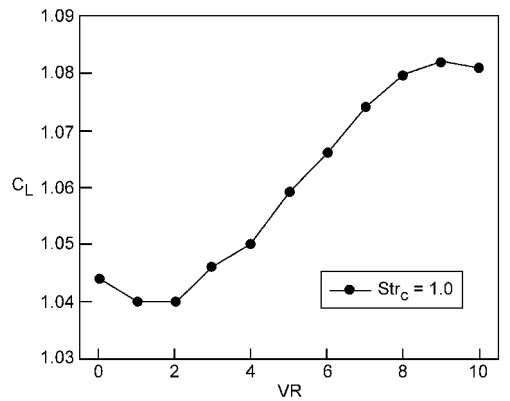

Fig. 6 Effect of jet pulse amplitude on lift enhancement with PVGJs for U_∞ = 66 m/s: α = 25 deg, δ_{le} = 30 deg.

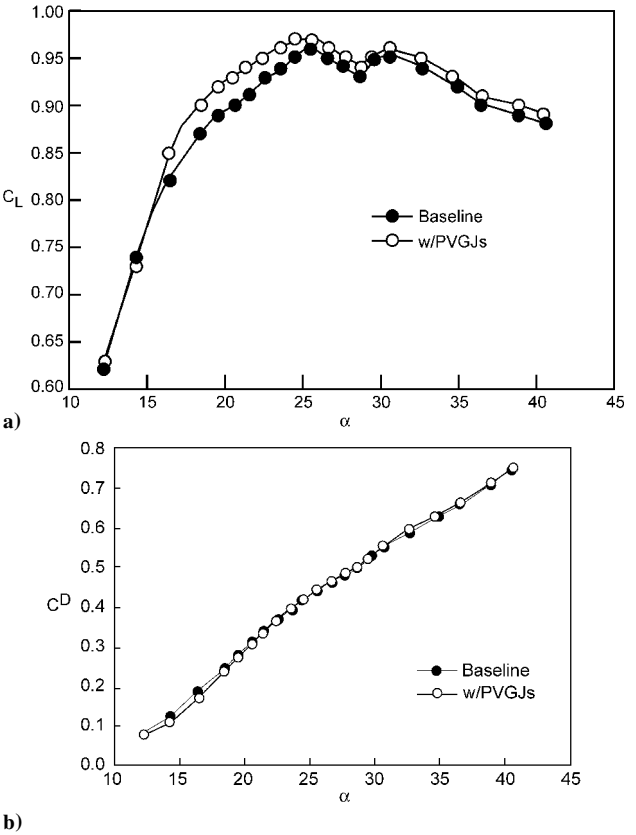

Fig. 7 Effect of PVGJs on lambda-wing model aerodynamic performance: U_∞ = 66 m/s, δ_{le} = 15 deg, δ_{te} = 0 deg; pulse conditions: Sr_c = 1.0, VR = 10; a) lift coefficient; b) drag coefficient.

Figure 7 shows lift and drag curves for the first PVGJ α-sweep test configuration along with the baseline curves for comparison. The freestream velocity for this case was $U_\infty = 66$ m/s. The jet pulse conditions were chosen based on the results from the new pulse parameter optimization studies discussed above. The jet pulse frequency was chosen to obtain a chord Strouhal number of $Sr_c = 1.0$, and the pulse amplitude corresponded to $VR = 10$. The blowing momentum coefficient for this condition was $C_\mu = 0.005$. The lift curve in Fig. 7a indicates that the use of PVGJs results in a lift enhancement over the range of $16 \leq \alpha \leq 40$ deg. Maximum lift increments lie in the range of $16 \leq \alpha \leq 25$ deg and are on the order of 3.5% of the baseline values although $C_{L\,\max}$ only increases about 1%. The drag curves in Fig. 7b show that the use of pulsed blowing does not adversely affect drag over the entire α range investigated. Although the results are not shown here, it was found that the other forces and moments acting about the model axes were not significantly affected with the application of the PVGJs.

With a more extreme leading-edge flap deflection angle, $\delta_{le} = 30$ deg, the region of maximum lift increment from using PVGJs shifts to higher values of α (Fig. 8a). In this example, the use of leading-edge pulsed blowing results in an increase in $C_{L\,\max}$ of approximately 7%, again with a negligible change in the drag force produced. In addition to increasing the value of $C_{L\,\max}$, the use of PVGJs causes the lift curve to contain a sharper peak for this flap configuration, indicating more abrupt flow separation and stall with increasing α.

The results of using PVGJs for lift enhancement with the model in a high lift configuration ($\delta_{le} = 30$ deg, $\delta_{te} = 15$ deg) are shown in Fig. 9. This test was run with a freestream velocity $U_\infty = 33$ m/s. In this example, the addition of pulsed blowing allows the model

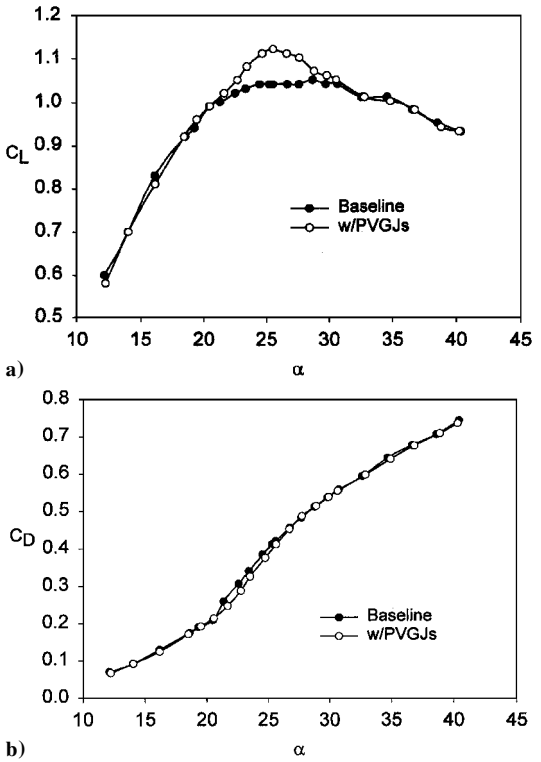

Fig. 8 Effect of PVGJs on lambda-wing model aerodynamic performance: U_∞ = 66 m/s, δ_{le} = 30 deg, δ_{te} = 0 deg; pulse conditions: Sr_c = 1.0, VR = 10; a) lift coefficient; b) drag coefficient.

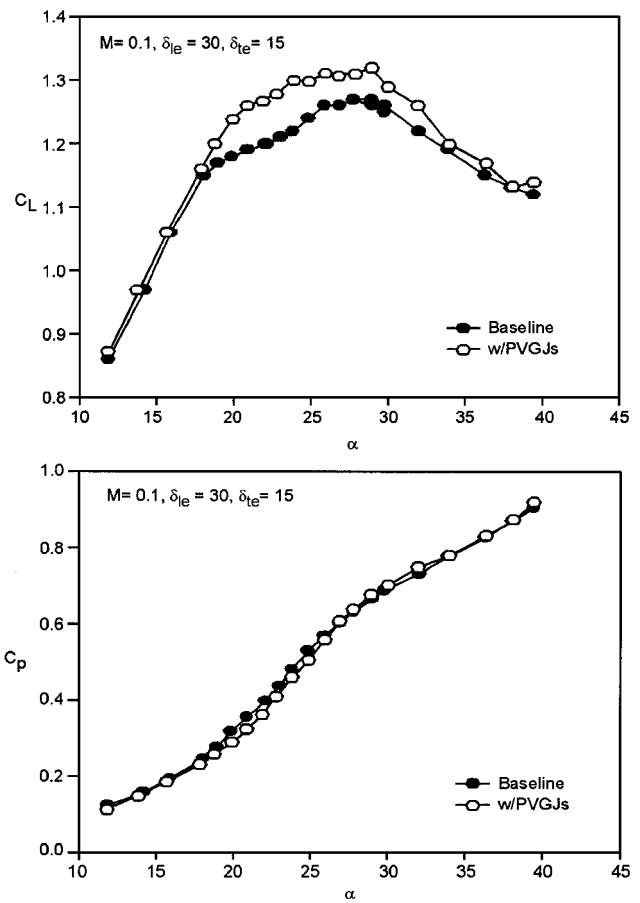

Fig. 9 Effect of PVGJs on lambda-wing model aerodynamic performance (high lift configuration): δ_{le} = 30 deg, δ_{te} = 15 deg; pulse conditions: Sr_c = 1.0, VR = 20.

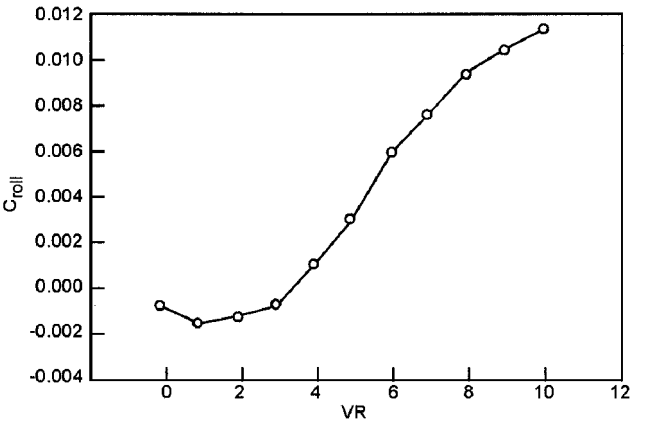

Fig. 10 Effect of single-wing application of PVGJs on lambda-wing model rolling moment coefficient: M_∞ = 0.2, α = 25 deg, δ_{le} = 30 deg, δ_{te} = 0 deg; pulse conditions: Sr_c = 1.0.

to maintain a linear lift curve for several degrees α in excess of where the baseline lift curve begins to roll over. For $20 \leq \alpha \leq 30$ deg, the average lift increment is on the order of 5% and improvements are realized over a range of approximately 23 deg. The jets increase $C_{L\,\max}$ by about 4.5%. Figure 9 also indicates a drag reduction over the range of $18 \leq \alpha \leq 26$ deg and this corresponds to the region where lift increments were maximum. These effects combine to create maximum increases in lift-to-drag ratios of approximately 17% when using PVGJs.

Effects of Asymmetric Pulsed Blowing on Model Rolling Moment

Tests were conducted to determine the effects of activating PVGJs on a single wing of the model to determine the feasibility of using the flow-control system to effect rolling moments at high α. Figure 10 shows an example of the effect of increasing the pulse intensity on the rolling moment coefficient, C_{roll}. The model configuration in this example is with leading-edge flap deflection only ($\delta_{le} = 30$ deg) and with $\alpha = 25$ deg. The freestream velocity was 66 m/s and the jet pulse Strouhal number was equal to 1.0.

The data indicate that above $VR = 2$, by increasing the pulse intensity in single-side blowing, a monotonic increase in C_{roll} can be produced. This result suggests that PVGJs may be used for improving high-α maneuverability in situations where conventional control surfaces may become ineffective as a result of separated flow. A reversed rolling moment appears at low velocity ratios, consistent with the results presented in Fig. 6 and discussed above.

Transonic Wing Experiments

Airfoil Section Model

The airfoil used in the transonic wind tunnel experiments was a modified SP215 with a 25% chord flap at the leading edge. The model, shown in Fig. 11, had a 15.2 cm chord and was instrumented with an array of 85 pressure taps as shown. The model was cast from a high-strength epoxy containing carbon fibers. The main element and the flap were supported by end blocks that are inserted into rotating plugs in the wind-tunnel wall, providing a means of changing angle of attack and flap angle.

The leading-edge flap was fitted with two pulsed jets for separation control. Flow to the jets was supplied by a rotating valve embedded in the model leading edge. The valve was capable of supplying 4.5 g/s of air to each jet. Flow nozzles embedded in the valve and situated at the airfoil surface expanded the flow to M 3.5 at the jet exit. The jet nozzles were pitched and rolled with respect to the model chord line at 90 and 45 deg, respectively (see Fig. 11).

Valve Performance Measurement

A series of flow measurements evaluated the performance of the pulsed valve. A piezoelectric pressure transducer fitted with a small-diameter pitot probe was used to measure jet exit velocities. Because the piezoelectric transducer was not capable of measuring

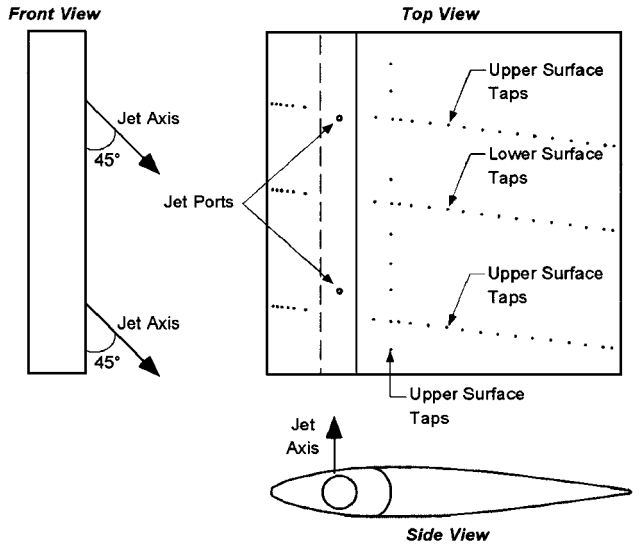

Fig. 11 SP215 airfoil section used in compressible flow experiments.

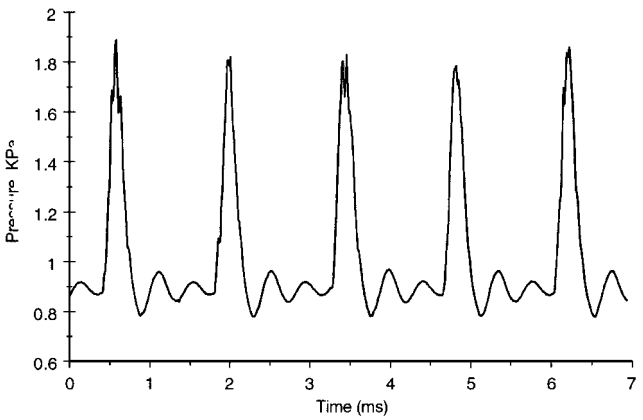

Fig. 12 Stagnation pressure measurements at exit of high-speed model pulsed valve.

steady pressures, a dial pressure indicator was also used to determine mean jet dynamic pressures. This mean was then added to the value measured by the piezoelectric transducer to obtain the actual pressure. The signal from the piezoelectric transducer was sampled using a high-speed data acquisition system at 71.68 kHz. Figure 12 plots a train of jet pulses for which the pressure inside the valve was 2.8 MPa. The signal exhibits a ringing, a result of the dynamics of the transducer. However, the pulse shape, a high, narrow peak, is clearly represented. Because of complexities in the flowfield, it is difficult to correlate the stagnation pressures measured from the probe to exit velocities. However, if it is assumed that the flow is fully developed at the peak of the pulse profile and a normal shock stands in front of the probe, the calculated peak exit Mach number is $M = 3.45$.

High-Speed Facility

High-speed experiments were conducted in the 6×22 in. blowdown transonic wind tunnel at the Ohio State University Aeronautical and Astronautical Research Laboratory. The experiments described below were performed in the range of $0.3 \leq M_\infty \leq 0.5$. The tunnel is driven from pressurized tanks, and a settling chamber with flow conditioning screens precedes the test section. To achieve realistic flight Reynolds numbers, the test section was operated above atmospheric pressure, with typical static pressures ranging from 30–40 psia depending on the freestream Mach number.

The wind tunnel is equipped with a wake velocity probe and a pressure-scanning system to assess airfoil performance. The wake probe traverses the test section vertically and is used to measure the airfoil wake velocity profile to determine drag. The pressure-scanning system measures upper- and lower-surface static pressure distributions on the test airfoil from pressure tap arrays. It incorporates a guillotine mechanism to sample and lock the pressure from each tap during the course of a test run. A Scanivalve then scans the channels, and a pressure transducer measures each of the stored pressures after the run is completed. The duration of each experimental run was approximately 10 s.

Discussion of High-Speed Test Results

Separation control experiments were performed over the Mach number range of $0.3 \leq M_\infty \leq 0.5$. Lift and drag performance curves were constructed for conditions with and without pulsed jets for several model parameter variations. The parameters that were varied include free stream Mach number, angle of attack, and leading-edge flap deflection angle, δ_{le}. The effectiveness of the pulsed jets in controlling separation and enhancing airfoil performance was assessed for cases with and without transonic flow occurring over the upper surface of the model.

The critical Mach number, M_{cr}, defined as the freestream Mach number that results in the airfoil upper-surface flow accelerating to the local sonic velocity, is dependent on the leading-edge flap deflection angle and the airfoil angle of attack. Flap deflection angles of $\delta_{le} = 5$, 15, and 30 deg were used in the present experiments and supercritical flow regions were observed for $M_\infty \geq 0.4$ for several values of α.

Lift and drag forces served as metrics for assessing the effects of PVGJs on airfoil performance. The lift was computed by integrating the pressure distribution measured from the taps. Drag was computed by integrating the wake velocity profile and computing the change in momentum across the test section using the freestream density and assuming the upstream flow is uniform across the test section.

The first set of experiments measured baseline (no pulsed jets) lift and drag curves for the airfoil model for freestream Mach numbers of $M_\infty = 0.3$, 0.4, and 0.5. The lift curves are shown in Fig. 13a. With a leading-edge flap deflection angle of 15 deg, the airfoil displays similar performance for the $M_\infty = 0.3$ and 0.4 cases with a value of $C_{\ell\,\max} \approx 1.35$ occuring at $\alpha = 15$ deg, although the $M_\infty = 0.4$ case stalls slightly before the $M_\infty = 0.3$ case. The curve for $M_\infty = 0.5$

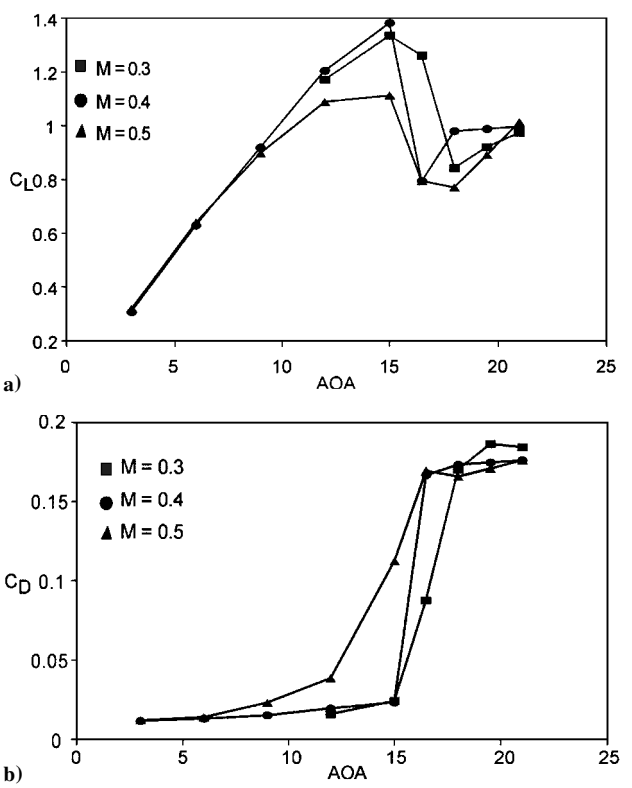

Fig. 13 Aerodynamic lift characteristics for SP215 airfoil without pulsed jets: δ_{le} = 15 deg; a) lift coefficient; b) drag coefficient.

shows an earlier roll off in lift with a value of $C_{\ell\max} \approx 1.1$. There is a trend toward earlier stall with increasing Mach number. This behavior is consistent with the occurrence of supercritical flow over the upper surface, as was evidenced by the measured pressure distributions for the $M_\infty = 0.5$ case. In all cases, the lift decreases above the stall angle for several degrees and then begins to rise again as a result of increased lift on the leading-edge flap region.

The drag curves for the $M_\infty = 0.3$ and 0.4 cases (Fig. 13b) show a sharp increase for $\alpha > 15$ deg, whereas the supercritical flow case ($M_\infty = 0.5$) exhibits significant drag increases at lower angles of attack ($\alpha > 6$ deg). This large increase at low α is due to the wave drag associated with shock formation over the upper surface of the airfoil. The drop in lift and increase in drag for increasing angle of attack is a result of flow separation over the airfoil upper surface.

Once the airfoil's inherent behavior had been quantified, the jets were operated to determine their effect on the lift and drag characteristics. The effects of using pulsed jet separation control on airfoil performance were quantified by comparing the baseline lift and drag with that measured with pulsed jets on. Figures 14–16 compare the airfoil performance with pulsed jets to that of the baseline case for three Mach numbers. During these experiments, the pulsed jets were operated at a fixed Strouhal number of $Sr_c = 0.45$ with the pulse frequency adjusted for different freestream Mach numbers. The pulsed jet mass-flow rate was held fixed at approximately 4.5 g/s to each jet, corresponding to a jet velocity ratio $VR = 10$, 8, and 6 and a momentum coefficient of $C_\mu = 0.01, 0.006$, and 0.004 for $M = 0.3$, 0.4, and 0.5, respectively.

The first plot in each of Figs. 14–16 depicts the effects of pulsed jets on airfoil section lift. The results indicate that the jets produce an increase in lift in the post-stall region. The jets exhibited maximum levels of lift enhancement for the subcritical case ($M_\infty = 0.3$). For the two larger flap deflection angles, the jets delay stall to angles of attack 3–4 deg higher than the baseline case. The result is an increase in $C_{\ell\max}$ of 9% for $\delta_{le} = 5$ deg and 11% for $\delta_{le} = 30$ deg. In the $\delta_{le} = 15$ deg case, the increase in $C_{\ell\max}$ is smaller (about 3.5%),

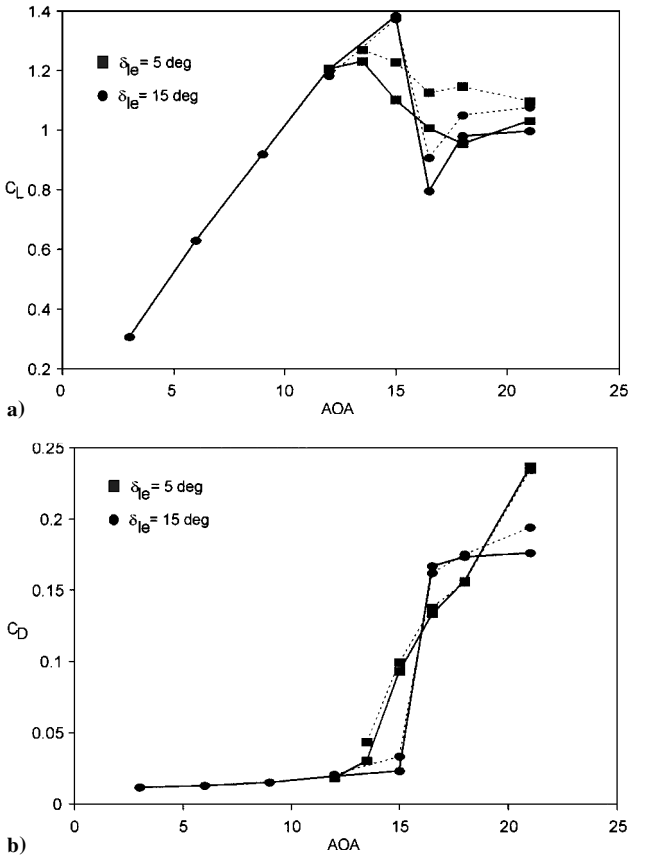

Fig. 15 Effect of PVGJs on SP215 aerodynamic characteristics with M_∞ = 0.4 and for two different leading-edge flap deflections. Jet pulse conditions: f_p = 388 Hz, VR = 4.7: a) lift coefficient; b) drag coefficient (dashed line denotes cases with pulsed jets).

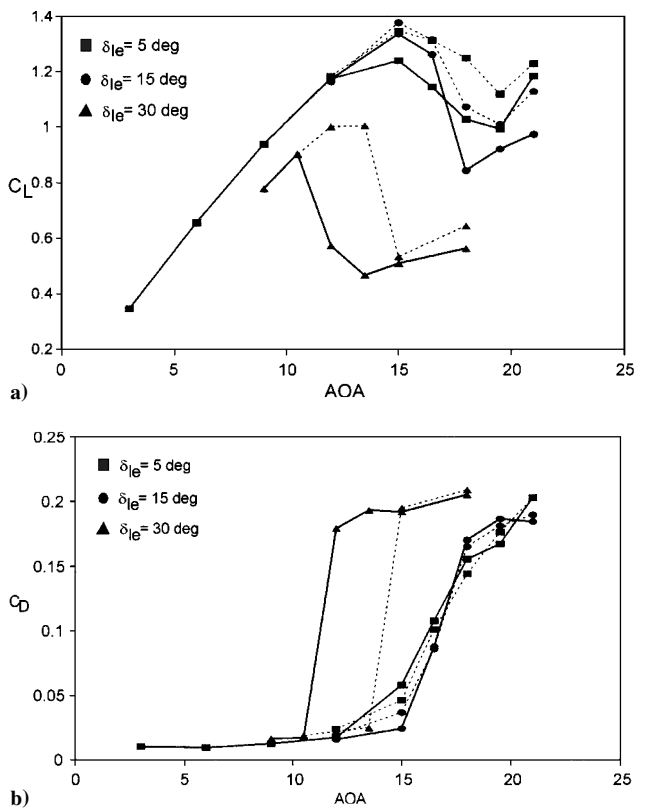

Fig. 14 Effect of PVGJs on SP215 aerodynamic characteristics with M_∞ = 0.3 and for three different leading-edge flap deflections. Jet pulse conditions: f_p = 290 Hz, VR = 6: a) lift coefficient; b) drag coefficient (dashed line denotes cases with pulsed jets).

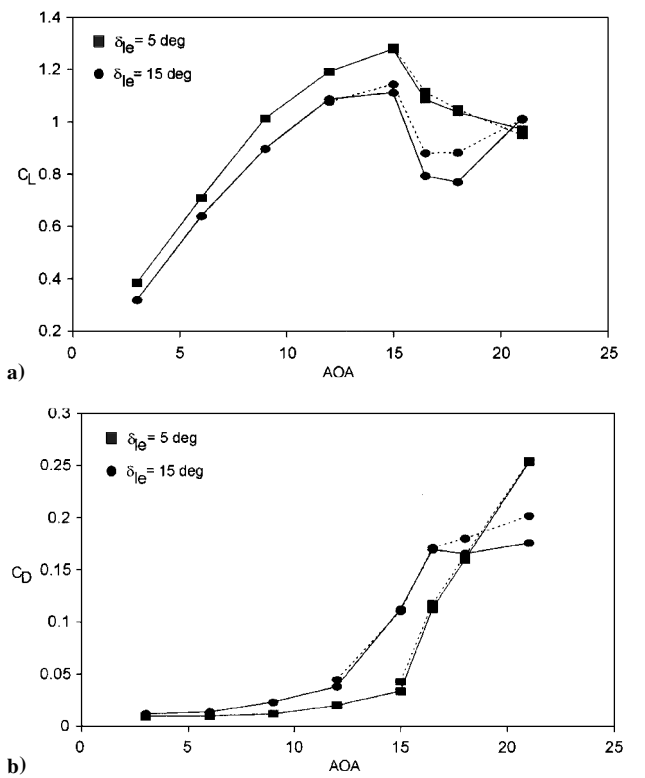

Fig. 16 Effect of PVGJs on SP215 aerodynamic characteristics with M_∞ = 0.5 and for two different leading-edge flap deflections. Jet pulse conditions: f_p = 486 Hz, VR = 3.7: a) lift coefficient; b) drag coefficient (dashed line denotes cases with pulsed jets).

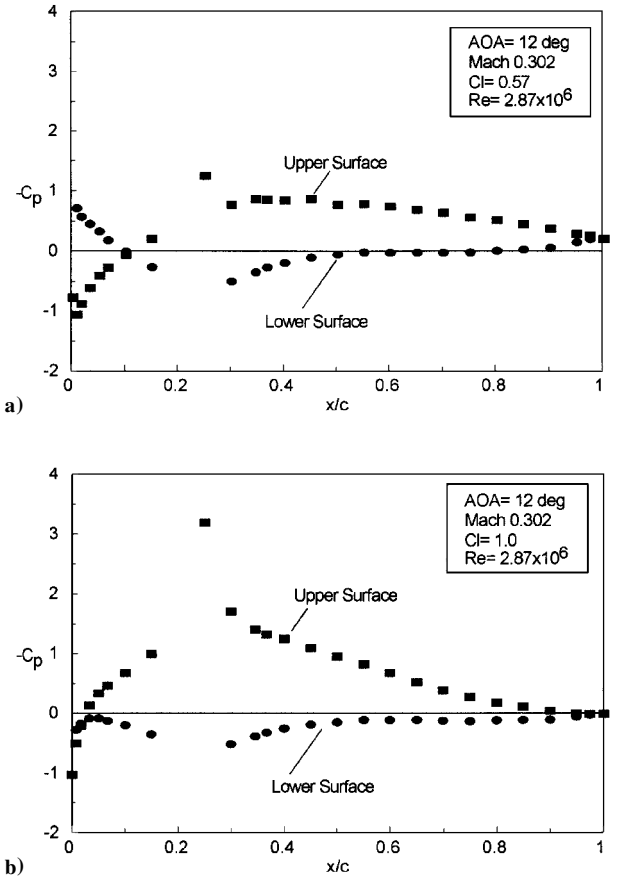

Fig. 17 Surface pressure and wake profile data from SP215 airfoil; M_∞ = 0.3, α = 12 deg, δ_{le} = 30 deg; a) baseline (no pulsed jets); b) with pulsed jets, f_p = 229 Hz, VR = 6.

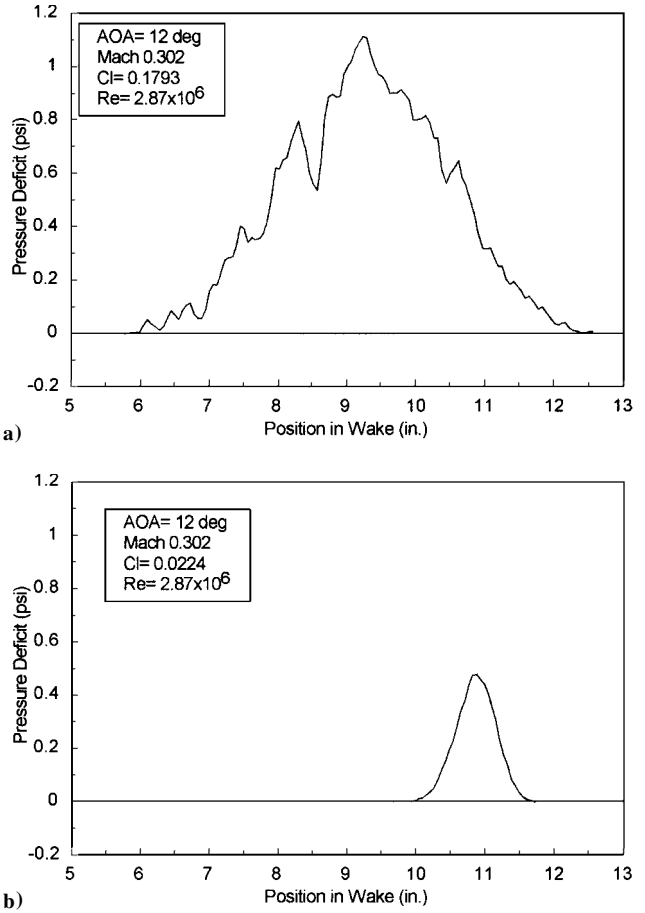

Fig. 18 Surface pressure and wake profile data from SP215 airfoil; M_∞ = 0.3, α = 12 deg, δ_{le} = 30 deg; a) baseline (no pulsed jets); b) with pulsed jets, f_p = 229 Hz, VR = 6.

but the jets produce much larger increases in lift throughout the post-stall region.

In the higher-speed cases, $M = 0.4$ and 0.5, the jets produce smaller lift increases. At $M = 0.4$, they improve lift only at $\delta_{le} = 5$ deg. At $M = 0.5$, the trend is reversed, with improvement only at $\delta_{le} = 15$ deg. In both cases, changes to $C_{\ell\,max}$ are small, and the largest increases in C_ℓ are in the deep stall regime.

The second plot in each of Figs. 14–16 show the drag on the airfoil as a function of α for $M_\infty = 0.3$–0.5, with and without jets. The most notable change in drag appears for the case that also provided the greatest lift improvement: $M = 0.3/\delta_{le} = 30$ deg. Here the stall, and hence the drag rise, is delayed by 3 deg.

The other conditions exhibit very small changes in drag. The jets in fact increase drag slightly for all other cases except one, $M = 0.3/\delta_{le} = 0.5$, where they decrease drag slightly.

The lift plots just described show that the highest lift increases are made for the highest flap-deflection angles. This is because at large leading-edge deflections, the separation occurs near the hinge line and downstream of the jets rather than near the leading edge. The jets are most effective when they generate the mixing structures ahead of the separation point.

Evidence that the jets increase lift, at least in the subcritical case, by preventing separation can be found in Figs. 17 and 18. Figure 17 compares the pressure distribution on the airfoil for two cases: one with and one without jets. The pressure distribution in Fig. 17a exhibits a weak suction peak and flat upper-surface pressure profile consistent with airfoil stall. Figure 17b indicates that the leading-edge pressure peak is restored with the use of the pulsed jets, showing that the jets have suppressed the separation from the upper surface.

Figure 18 shows the wake velocity measurements for the same cases as shown in Fig. 17. In the baseline plot (Fig. 18a), the wake velocity deficit is broad and irregular, consistent with expectations for the wake of a stalled airfoil. Figure 18b shows a narrow, smooth wake velocity profile, indicating that the jets have indeed reattached the flow.

Accuracy of Experimental Measurements

Estimates of the uncertainty in these experimental measurements are based on information provided by the operators of the wind tunnel. For the lambda-wing experiments, the primary experimental instrument was the force balance, which can measure forces to within 4.5N (1 lb). For the lambda-wing model, these uncertainties correspond to aggregate coefficient uncertainties of 0.07 at a freestream velocity of 33 m/s, and 0.04 at 66 m/s.

Primary measurements in the high-speed experiments were of the wing pressures and the downstream dynamic pressure. The pressure transducers had an accuracy better than 25 Pa. Integrating the error over the upper and lower wing surface provides an estimated lift coefficient error of 0.005 at $M = 0.3$.

Summary

The experiments described were designed to investigate the usefulness of PVGJs on configurations relevant to aircraft. The pulsed jet devices were first evaluated for low-speed, high-α flight of an advanced fighter configuration, the lambda wing. The tests were then extended to higher speeds to show that the jets may be useful in conditions relevant to transonic cruise.

The lambda-wing tests showed that the jets can increase lift and decrease drag at high angles of attack, offering improved post-stall maneuver performance. The jets produced peak lift increases as high as 7%. In addition, the jets can be operated asymmetrically to provide lateral maneuvering control in this region where conventional control surfaces have reduced effectiveness. The variation in effectiveness with velocity ratio further endorses the use of PVGJs for lateral directional control.

The transonic airfoil tests showed that the jets are very effective just below critical conditions and, although their effectiveness is reduced, show some ability to suppress separation at supercritical speeds. There, effect is to increase lift while causing only small changes in drag, resulting in an overall increase in lift-to-drag ratio. The improvements at low speeds may be used to reduce takeoff or landing speeds. The lift increases in the higher-speed cases, although small, indicate that the jets may be useful for preventing separation induced by hinge line shocks at transonic speeds.

The jet design parameters were all based on earlier low-speed experiments with plates and airfoil sections. The lambda-wing tests provided an opportunity to explore the effect of parameter variation. The investigation revealed that the empirical scaling rules derived for the low-speed sections cannot be directly applied to swept and tapered wings using the mean aerodynamic chord. It is reasonable to think, then, that greater effects may be achieved in the transonic case with a better set of operating parameters. Unfortunately, the high speed test did not provide an opportunity to explore parameter effects. It may also be true that jet placement, particularly for the lambda wing, cannot be extended directly from the preliminary investigations. There were no geometry variations in any of the experiments described here, so no conclusions may be drawn on that matter.

The results show that PVGJs will be useful for aircraft configurations. Applications include improving high-α maneuvering for fighters, takeoff roll reduction, and reduction of lift-to-drag ratio for transonic cruise.

Conclusions

From the preceding discussion, we draw the following conclusions:

1) PVGJs increased lift and lift-to-drag ratio, while effecting only small changes to drag, for aircraft-relevant configurations. Demonstrations were conducted for both an advanced fighter configuration with swept wings and a transonic airfoil section relevant to cruise conditions.

2) In the airfoil section test, the effect of the jets was diminished at supercritical speeds.

3) The optimum operating parameters as determined from low-speed airfoil section and flat plate tests cannot be directly applied to swept and tapered wings using the mean aerodynamic chord as a reference length.

4) PVGJs are most effective at high leading-edge flap deflections.

Acknowledgments

This work was sponsored by the Flight Dynamics Directorate, Wright Laboratory, Air Force Material Command (AFMC), Wright Patterson Air Force Base, under the supervision of Kevin Langan (Contract F33615-94-C-3006). The authors would like to thank David Rossi for his help in designing and assembling the experimental apparatus and H. Legner, M. Allen, P. Joshi, and S. Davis for many helpful discussions.

References

[1]McManus, K. R., Legner, H. H., and Davis, S. J., "Pulsed Vortex Generator Jets for Active Control of Flow Separation," AIAA Paper 94-2218, June 1994.

[2]McManus, K. R., Joshi, P. B., Legner, H. H., and Davis, S. J., "Active Control of Aerodynamic Stall Using Pulsed Jet Actuators," AIAA Paper 95-2187, June 1995.

[3]McManus, K. R., Ducharme, A., Goldey, C., and Magill, J., "Pulsed Jet Actuators for Suppressing Flow Separation," AIAA Paper 96-0442, Jan. 1996.

[4]Barret, R., and Farokhi, S., "On the Aerodynamic Performance of Active Vortex Generators," AIAA Paper 93-3477, Aug. 1993.

[5]Klausmer, S., Papadakis, M., and Lin, J., "A Flow Physics Study of Vortex Generators on a Multi-Element Airfoil," AIAA Paper 96-0548 Jan. 1996.

[6]Lin, J., Robinson, S., McGhee, R., and Valarezo, V., "Separation Control on High-Lift Airfoils via Micro-Vortex Generators," *Journal of Aircraft*, Vol. 31, No. 6, 1994, pp. 1317–1329.

[7]Selby, G. V., Lin, J. C., and Howard, F. G., "Control of Low-Speed Turbulent Separated Flow Using Vortex Generator Jets," *Experiments in Fluids*, Vol. 12, 1992, pp. 394–400.

[8]Johnston, J., and Nishi, M., "Vortex Generator Jets: Means for Flow Separation Control," *AIAA Journal*, Vol. 28, No. 6, 1990, pp. 989–994.

[9]Johnston, J., "Pitched and Skewed Vortex Generator Jets for Control of Turbulent Boundary Layer Separation: A Review," SEDSM 99-6917, July 1999.

[10]Compton, D. A., and Johnston, J. P., "Streamwise Vortex Production by Pitched and Skewed Jets in a Turbulent Boundary Layer," *AIAA Journal*, Vol. 30, No. 3, 1992, p. 640.

[11]Zhang, X., Zhang, H., and Collins, M., "Some Aspects of Streamwise Vortex Production Using Air Jets," AIAA Paper 96-0209, Jan. 1996.

[12]Seifert, A., Bachar, T., Koss, D., Shepshelovich, M., and Wygnanski, I., "Oscillatory Blowing: A Tool to Delay Boundary Layer Separation," *AIAA Journal*, Vol. 31, No. 11, 1993, pp. 2052–2060.

[13]Wygnanski, I., and Seifert, A., "Control of Separation by Periodic Oscillation," AIAA Paper 94-2608, June 1994.

[14]Johari, H., and McManus, K. R., "Visualization of Pulsed Vortex Generator Jets for Active Control of Boundary Layer Separation," AIAA Paper 97-2021, June 1997.

[15]McManus, K. R., and Magill, J., "Separation Control in Incompressible and Compressible Flows Using Pulsed Jets," AIAA Paper 96-1948, June 1996.

[16]Seifert, A., and Pack, L., "Oscillatory Control of Separation at High Reynolds Numbers," AIAA Paper 98-0214, Jan. 1998.

[17]Suzuki, T., Nagata, M., Shizawa, T., and Honami, S., "Optimal Injection Condition of a Single Pulsed Vortex Generator Jet to Promote the Cross-Stream Mixing," *Experimental Thermal and Fluid Science*, Vol. 17, 1998, pp. 139–146.